Revised paper submitted to *GEODERMA*

Thallium stable isotope ratios in naturally Tl-rich soils

Aleš Vaněk[1,*], Andreas Voegelin[2], Martin Mihaljevič[3], Vojtěch Ettler[3], Jakub Trubač[3], Petr Drahota[3], Maria Vaňková[3], Vendula Oborná[1], Kateřina Vejvodová[1], Vít Penížek[1], Lenka Pavlů[1], Ondřej Drábek[1], Petra Vokurková[1], Tereza Zádorová[1], Ondřej Holubík[1]

[1]Department of Soil Science and Soil Protection, Faculty of Agrobiology, Food and Natural Resources, Czech University of Life Sciences Prague, Kamýcká 129, 165 00 Prague 6, Czech Republic

[2]Eawag, Swiss Federal Institute of Aquatic Science and Technology, Ueberlandstrasse 133, CH-8600 Duebendorf, Switzerland

[3]Institute of Geochemistry, Mineralogy and Mineral Resources, Faculty of Science, Charles University, Albertov 6, 128 00 Prague 2, Czech Republic

* Phone: +420 224 382 752; Fax: +420 234 381 836; E-mail: vaneka@af.czu.cz

ABSTRACT

Soils on the Erzmatt (Switzerland) formed on hydrothermally mineralized dolomite rock and are naturally Tl-rich. In this study, we investigated if variations in the stable Tl isotope ratios in soil samples from different profiles can be linked to data on the extractability and speciation of soil Tl and whether the isotopic data allow drawing conclusions on the geochemical processes that affected Tl over the course of soil formation. In two soil profiles, we observed a marked accumulation of the heavy ^{205}Tl isotope in the B horizons, with ε^{205}Tl values that were up to 7 higher than in the underlying bedrock. This ^{205}Tl enrichment, however, was neither reflected in the speciation of Tl nor its chemical fractionation. Furthermore, exchangeable soil Tl in the B horizons was found to be much isotopically lighter than the bulk soil Tl. These findings suggest that the observed isotopic shift may be linked to cyclic Tl mobilization and immobilization processes over the period of rock weathering and soil formation. Oxidative Tl uptake by Mn-oxides associated with a ^{205}Tl enrichment, continuous weathering of the Tl(III)-containing phases, followed by a Tl(I) remobilization (leading to enrichment in ^{205}Tl) are suggested to be responsible for the binding of the heavy Tl isotope fraction into other phases, mainly illite (a dominant Tl host), which is not normally expected. Hence, our results show that the Tl isotopic fractionation data measured in a dynamic multi-phase (soil) system can potentially serve as a proxy for tracing redox-controlled processes, but their use for phase or the sorption process identification is much more complicated.

KEYWORDS: Soil; Thallium; Isotope Fractionation; Illite

GRAPHICAL ABSTRACT

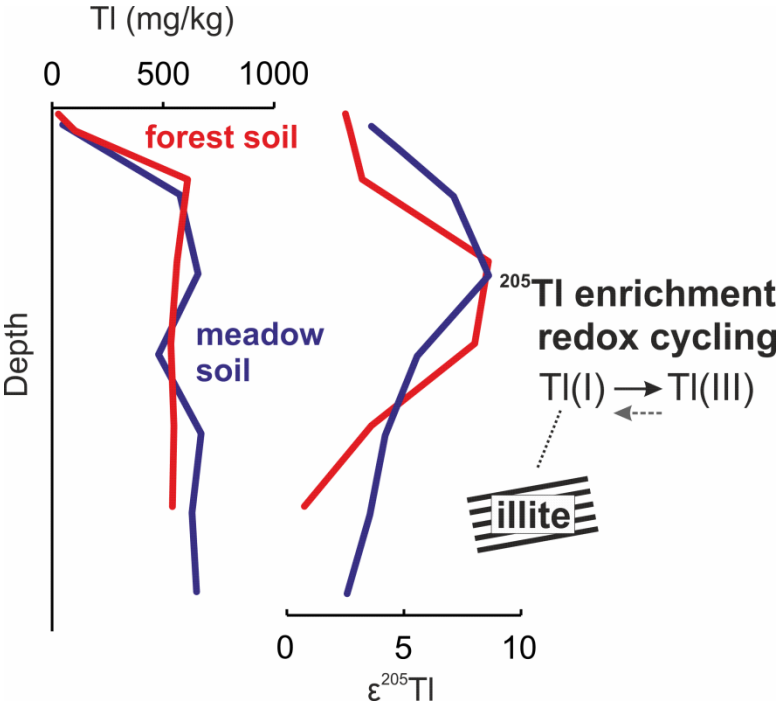

1. INTRODUCTION

Thallium (Tl) is a highly toxic trace element and contamination of environmental systems with Tl may represent a serious threat to human and environmental health. The geochemistry of Tl is complex. Monovalent Tl(I) tends to react as lithophile element in analogy to K, but exhibits also chalcophile character and can be bound to S in inorganic and organic compounds. Under highly oxidizing conditions, strongly hydrolyzing and poorly soluble Tl(III) may occur (Peter and Viraraghavan, 2005). Thallium has two stable isotopes, ^{203}Tl and ^{205}Tl, and variations in the stable Tl isotope ratios in soils and at the soil-plant interface may offer insights into the biogeochemical processes that control the environmental fate and impact of Tl (Howarth et al., 2018; Nielsen et al., 2017). In a pioneering study using high-resolution multi-collector inductively coupled plasma mass spectrometry (MC-ICP-MS), Kersten et al. (2014) demonstrated that stable Tl isotope ratios can be used to identify anthropogenic and geogenic Tl inputs into soil and that plants may preferentially accumulate the light ^{203}Tl in plants. Studies with plants grown in soil and hydroponic systems showed systematic plant-specific Tl isotope fractionation patterns, with preferential transfer of light ^{203}Tl from nutrient solutions to roots and further into stems and leaves, resulting in a decrease in the ε^{205}Tl along this transfer path. These isotopic trends were clearly due to Tl translocation and/or specific chemical reactions (Rader et al., 2019; Vaněk et al., 2019). In relation to rock weathering and soil formation, Howarth et al. (2018) showed that intensive weathering in laterite soil profiles may cause enrichment in ^{205}Tl, presumably due to redox/sorption processes and changes in mineralogy, where Tl(I) oxidation to Tl(III) by Mn-oxides is thought to be the key factor (Nielsen et al., 2013; Rehkämper et al., 2004). In relation to anthropogenic activities, we observed Tl isotopic fractionation during both industrial high-temperature processes (coal burning and metallurgy) and post-depositional Tl dynamics in soils, probably related to Tl sorption or (co)precipitation (Vaněk et al., 2016, 2018). Currently

97 available data thus suggest that variations in the Tl isotopic signature may act as a proxy for
98 specific geochemical and biological processes/reactions and associated enrichments or
99 chemical alterations of Tl. However, to advance the level of understanding of Tl isotopic
100 patterns in soil systems, information on stable Tl isotope ratios should be evaluated in
101 combination with data on the speciation and fractionation of Tl in soils.

102 In the Swiss Jura Mountains, soils on the Erzmatt ("ore meadow") contain
103 exceptionally high levels of geogenic Tl of up to several thousand mg/kg, due to soil
104 formation on dolomite rock that hosts weathered hydrothermal Tl-As-Fe sulfide
105 mineralization (Hermann et al., 2018; Voegelin et al., 2015). Using X-ray absorption
106 spectroscopy (XAS), it has been shown that secondary minerals from the weathered
107 mineralization, avicennite (Tl_2O_3) and Tl(I)-bearing jarosite, mainly occur in deeper soil
108 horizons (Voegelin et al., 2015). With respect to pedogenic Tl species, Tl(I) bound to illite (or
109 other micaceous clay minerals) represented the dominant Tl species, but also Tl(III) sorbed
110 onto Mn-oxides was identified (Voegelin et al., 2015).

111 The present study was performed to evaluate if variations in stable Tl isotope ratios in
112 soil samples from Erzmatt can be linked to data on the extractability and speciation of Tl and
113 whether the data allow drawing conclusions on the geochemical processes that affect Tl over
114 the course of soil formation. For this purpose, one soil profile was sampled on the Erzmatt
115 meadow and one in the adjacent forest. The samples were analyzed for basic soil chemical
116 and mineralogical properties, Tl fractionation (single and sequential batch extractions), Tl
117 speciation (XAS) and Tl isotope ratios (MC-ICP-MS). Data from the two soil profiles were
118 combined with the Tl isotope data on selected soil samples from an earlier study that exhibit
119 substantial variations in Tl speciation (Voegelin et al., 2015).

2. EXPERIMENTAL SECTION

2.1 General site description

The Erzmatt is a meadow situated near the village Buus in the Swiss Jura Mountains (Figure S1, Supplementary Material). The soils on the Erzmatt contain high levels of Tl, As and Fe due to their formation on the carbonate rock (lower Keuper, triassic dolomite) that locally hosts a weathered hydrothermal Tl-As-Fe mineralization (Hermann et al., 2018; Voegelin et al., 2015). The soils are characterized as Cambisols,with neutral to slightly acidic pH values and exhibit weak redoximorphic features (Voegelin et al., 2015). The Erzmatt site was used as a pasture in the past. In 2016, the agricultural use of the zone with the highest Tl contents has been discontinued and this land is now managed as an ecological compensation area (fallow with native wild herbs). The speciation of soil Tl and the mineralogy of secondary Tl- and As-bearing minerals in soil samples from the Erztmatt were studied in earlier work (Hermann et al., 2018; Voegelin et al., 2015).

2.2 Soil sample collection

Two soil profiles were sampled in this study, one at the meadow (M) and one under the adjacent forest (F) (Figures S1, S2 and S3, Supplementary Material). Soil samples and one bedrock sample (meadow profile) were collected from individual soil layers in ~1×1 m wide pits according to the soil development (1-5 cm). All soil samples were air-dried and sieved through a 2-mm stainless-steel sieve prior to further use/analyses. In addition to the soil samples from the two soil profiles, selected soil samples from that have previously been shown to exhibit large variations in Tl speciation (Voegelin et al., 2015) were analyzed for their stable Tl isotope ratios as well.

2.3 Soil sample characterization

145 The soil pH (active, exchangeable) was determined at a 1:5 (v/v) ratio of soil to H_2O
146 or 1 M KCl solution. Total carbon (TC) and total sulfur (TS) were identified by catalytic
147 oxidation using a Flash 2000 Series CNS analyzer (Thermo Scientific, Germany). The cation
148 exchange capacity (CEC) was determined by saturating soil cation exchange sites with Ba^{2+}
149 (0.1 M $BaCl_2$) followed by Ba^{2+} exchange with $MgSO_4$. The clay content was estimated by
150 the sedimentary method on mixed sample sets for each soil profile. X-ray diffraction (XRD)
151 data were collected using an X´Pert Pro diffractometer (PANalytical, the Netherlands) under
152 the following conditions: CuKα radiation, 40 kV, 30 mA, step scanning at 0.02º/150 s in the
153 range 3-80º 2θ. Mineral phases were identified using X'Pert HighScore software 1.0 and the
154 JCPDS PDF-2 database.
155 A single extraction with 1 M NH_4NO_3 at a solid to liquid ratio of 1:2.5 (2 h reaction
156 time) was used to quantify the exchangeable soil Tl fraction. The exchangeable Tl from
157 selected soil samples was also analyzed for its stable Tl isotope signature. Acid oxalate
158 extraction (0.2 M ammonium oxalate/oxalic acid at pH 3.0) (Pansu and Gautheyrou, 2006)
159 was used to quantify oxalate-extractable Fe and Mn and co-extracted Tl. A modified BCR
160 sequential extraction procedure by Rauret et al. (2000) was employed to quantify chemical
161 fractionation of Tl (and Mn) in four extraction steps (with hypothetical interpretation in
162 parentheses): (i) 0.11 M CH_3COOH, pH 3 (acid-extractable); (ii) 0.5 M $NH_2OH{\cdot}HCl$, pH 1.5
163 (reducible); (iii) 8.8 M H_2O_2/1 M CH_3COONH_4, pH 2 (oxidizable); (iv) hot acid digestion
164 with HNO_3/HCl/HF (residual). Analytical grade chemicals (Lach-Ner, Czech Republic) were
165 used for all the extractions.
166 To characterize the speciation of Tl in selected samples (Oi, Oe, Ah, Bw2 and C
167 layers/horizons), the dried and powdered samples were prepared as 7-mm pellets for analysis
168 by Tl L_{III}-edge X-ray absorption near-edge structure (XANES) spectroscopy at the SuperXAS
169 beamline at the Swiss Light Source (SLS, Villigen, PSI), using the same setup as in previous

works (Vaněk et al., 2018; Wick et al., 2018). The XANES spectra were evaluated by linear combination fitting based on selected reference spectra. Starting from the best one-component fit, fits with more components were considered only if the sum of the squared residuals of the fit decreased by at least 10% (relative). The sum of the fitted fractions was not constrained.

To determine the total element concentrations and Tl isotopic fractionation, the samples were homogenized and finely ground in an agate mill. A mass of 0.2 g of each sample was decomposed using a mixture of concentrated acids. Nitric and HF acids mixed in a ratio of 2:1 were added to the sample in a total volume of ≤20 mL; the dissolution was performed in 60-mL PTFE beakers (Savillex, USA) on a hot plate (150 °C) for 48 h with the subsequent addition of 2-4 mL of H_2O_2 for possible organic residues.

The element concentrations in all the digests and soil extracts were measured in triplicate using either inductively coupled plasma optical emission spectrometry (ICP-OES, iCAP 6500, Thermo Scientific, UK) or quadrupole based inductively coupled plasma mass spectrometry (Q-ICP-MS, Xseries II, Thermo Scientific, Germany). The standard reference material NIST 2711 (Montana Soil) (National Institute of Standards and Technology, USA) was used for QC (Table S1, Supplementary Material).

2.4 Thallium isotope separation

Thallium was isolated from the sample matrix using chromatographic separation with an anion exchange resin (Bio-Rad AG1-X8, 200-400 mesh, Cl^- cycle) as earlier described in detail (Baker et al., 2009; Vaněk et al., 2016, 2018). The only exception for this work was the absence of HBr in all the chromatographic stages. The obtained Tl/Pb fraction after the first extraction step was evaporated and redissolved in 0.1 M HCl to be ready for the next part of the Tl purification. Once the final Tl fraction (with no Pb present) was obtained, the Tl sample

was transferred to 2% HNO_3. Suprapure chemicals (Merck, Germany) and deionized water (MilliQ+, Millipore, USA) were employed during whole separation procedure.

2.5 Thallium isotope analysis

The MC-ICP-MS (Neptune Plus, Thermo Scientific, Germany) with a desolvating nebulizer (Aridus II, CETAC, USA) was used to measure the Tl isotope ratios. All the solutions were measured in 3 runs of 50 cycles. External normalization and standard sample bracketing (NIST SRM 997) were employed to eliminate the mass bias drift. For inter-element correction, the $^{208}Pb/^{206}Pb$ ratio was used to correct the raw $^{205}Tl/^{203}Tl$ ratio. The Tl isotopic composition was calculated using the following equation with □ notation relative to NIST SRM 997 (Eq. 1).

$$\varepsilon^{205}Tl = \frac{^{205}Tl/^{203}Tl_{sample} - ^{205}Tl/^{203}Tl_{NIST997}}{^{205}Tl/^{203}Tl_{NIST997}} \times 10^4 \quad (1)$$

Repeated analyses of the Sigma-Aldrich standard solution (for ICP analysis) with the mean of $\varepsilon^{205}Tl$ between -0.80 and -0.90 (n = 4) were consistent with the reported $\varepsilon^{205}Tl$ value (-0.81) (Prytulak et al., 2013). The external reproducibility had a value of ±0.7 $\varepsilon^{205}Tl$ (2 SD), based on long-term separate analyses (3 for this study) of standard reference material AGV-2 (Andesite, USGS, USA) in the same laboratory (Table S2, Supplementary Material), accounting for complete isotope analysis (sample dissolution, ion exchange chromatography and the mass spectrometric procedure).

3. RESULTS AND DISCUSSION

3.1 Characterization of soil profiles

The studied soils were classified as Eutric Cambisols (Figures S2 and S3, Supplementary Material). Key physicochemical properties are summarized in Table S3 (Supplementary Material). The soils can be briefly characterized by a medium content of clay fraction (12-15%), increased CEC of the mineral soil horizons (~30 cmol(+)/kg) and a circum-neutral pH value. The organic horizons contain up to 40 wt.% of TC, compared to only ~3% in the mineral horizons. The bulk soil mineralogy as determined by XRD is dominated by quartz (SiO_2), K-feldspar ($KAlSi_3O_8$), muscovite ($K,Al_2(AlSi_3O_{10})(F,OH)_2$) and/or illite ($(K,H_3O)Al_2(Si,Al)_4O_{10}(OH)_2$), chlorite and mixed-layered illite/smectite (Figure S4, Supplementary Material), in accordance with earlier mineralogical results (Hermann et al., 2018; Voegelin et al., 2015).

3.2 Total and extractable Tl in soil profiles

The depth profiles for total Tl, exchangeable Tl, oxalate-extractable Tl and the fractions of the sequential extraction are all shown in Figure 1 and Tables 1 and S4 (Supplementary Material). In both profiles, the Tl contents were the lowest in the topsoils (~20-200 mg Tl/kg) and increased to ~500-600 mg/kg with depth. The highest fractions of exchangeable and oxalate-extractable Tl were observed in the organic (O) horizons. In combination, these results pointed to the sorption of Tl on soil organic matter (SOM) in a relatively labile form. In the Ah and Bw horizons, only ~5% of the total Tl was exchangeable and ~7% oxalate-extractable. In the sequential extraction, most of the Tl was associated with the residual phase (Figure 1), in accordance with earlier studies on soil Tl fractionation in soils, sediments or waste materials (Aguilar-Carrillo et al., 2018; Gomez-Gonzalez et al., 2015; Grösslová et al., 2018; Jakubowska et al., 2007; Karbowska et al., 2014; Liu et al.,

2016, 2019). In agreement with the large fractions of exchangeable and oxalate-extractable Tl, the largest non-residual Tl fractions were observed in the O horizons. In the Ah and Bw horizons of both profiles, ~90% of the Tl was associated with the residual fraction, ~8% with the reducible fraction, and only minor percentages with the acid-extractable and oxidizable fractions, with a small peak for the topsoils (Oi layers) (Figure 1 and Table S5, Supplementary Material). Considering the speciation data from an earlier study on the Erzmatt site (Voegelin et al., 2015), and the XANES results provided below (indicating that most Tl in the two soil profiles studied here was associated with micaceous clay minerals), residual Tl in the Ah and Bw horizons probably mostly corresponds to Tl(I) in the interlayers of illite or other micaceous clay minerals. The minor fraction of Tl extracted in the reducible fraction of the sequential extraction may at least partly be Tl(I) or Tl(III) associated with soil Mn-oxides. Molar Tl/Mn ratios from the oxalate extraction (~0.01) and the reducible fractions (~0.02) (Table S4, Supplementary Material) thus point to high Tl loading of Mn-oxides, although it should be noted that both extracts could also mobilize variable proportions of exchangeable Tl (oxalate-extract without prior extraction of exchangeable Tl) or of Tl associated with mica-type minerals (hydroxylamine extract at pH 1.5) (Vaněk et al., 2010).

3.3 Thallium speciation in soil profiles

The Tl L_{III}-edge XANES spectra of selected samples from the soil profile under the meadow are shown in Figure 2, in comparison with the reference spectra of avicennite (Tl_2O_3) (proxy for Tl(III) in avicennite, adsorbed on Mn-oxides, or organically complexed), aqueous Tl^+ (proxy for (mostly hydrated) Tl(I) adsorbed on the soil minerals or organic matter or in the biomass), and Tl^+ adsorbed at the frayed edges of illite (proxy for dehydrated Tl^+ associated with micaceous clay minerals).

All the soil spectra indicated a clear prevalence of Tl(I) over Tl(III). The spectra of the two organic topsoil samples from the meadow, M-Oi and M-Oe, differed markedly from the spectra of the Ah, Bw and C horizons, and more closely resembled the spectrum of aqueous Tl^+, pointing to a larger fraction of Tl^+ adsorbed on the SOM or associated with the biomass (Vaněk et al., 2019; Wick et al., 2018). The spectra of samples M-Ah, M-Bw2 and M-C resembled the spectrum of Tl^+ adsorbed on illite, but exhibited more pronounced oscillations in the post-edge region than the illite reference spectrum. Considering that less than 10% of the Tl in these soil horizons was bound in exchangeable form (Table 1), we attribute this spectral difference to the presence of non-exchangeable structural Tl in the interlayers of micaceous clay minerals (Voegelin et al., 2015). For quantitative evaluation of the sample spectra by linear combination fitting (LCF), the spectrum of the soil sample M-C rather than the reference spectrum of Tl(I) adsorbed on illite was used to represent Tl associated with micaceous clay minerals. The LCF results (Table 2) pointed to a minor fraction of Tl(III) in the M-Oi sample, possibly organically-complexed Tl(III), in addition to Tl(I). In the Ah and Bw horizons, no species other than Tl(I) associated with micaceous clay minerals were detected by LCF, pointing to nearly uniform Tl speciation. The LCF analysis of the samples from the forest profile revealed only a minor fraction of hydrated Tl^+ in sample F-Oi, whereas Tl in all the other samples (F-Oe, F-Ah, F-Bw2, F-C) appeared to be mainly associated with micaceous clay minerals (Figure S5, Supplementary Material).

Overall, the spectroscopic results were in agreement with the chemical extractions. The large fractions of residual Tl in sequential extraction of the Ah, Bw and C horizon samples can be attributed to Tl incorporated into the interlayers of micaceous clay minerals (mainly illite); the exchangeable Tl can be interpreted at least partly as Tl adsorbed at the frayed edges of the clay minerals. The increases in the percentages of exchangeable Tl and Tl extracted by H_2O_2 in the organic topsoil samples are in accordance with the detectable

fractions of hydrated Tl^+ in LCF and point to the binding of Tl(I) by SOM and probably also association of Tl(I) with the living or dead biomass.

In comparison with the soil samples from the meadow/forest profiles, the soil samples from an earlier study on the Erzmatt site (Voegelin et al., 2015) spanned a wider range in soil Tl contents and Tl speciation (Table 3), with up to ~6000 mg Tl/kg, and containing all Tl(I) associated with illite, Tl(I)-jarosite, Tl(III) species like Tl_2O_3 or some other/unidentified Tl(III)-phases.

3.4 Stable Tl isotope ratios in soil samples

The Tl isotopic data for the meadow and forest soil profiles are listed in Table 1 and shown in Figure 1. The two soil profiles exhibited very similar trends in $\varepsilon^{205}Tl$ over depth. The lowest $\varepsilon^{205}Tl$ values of +0.8 to +2.6 were observed for the bottom C horizons of both soil profiles and the bedrock sample from the meadow profile. The value of $\varepsilon^{205}Tl$ gradually increased to +8.7 from the C horizons to the uppermost Bw horizons. The value of $\varepsilon^{205}Tl$ then decreased to +2.5 from the Bw over the Ah horizon to the overlying O horizons. The increase in $\varepsilon^{205}Tl$ from the C to the Bw horizons was not reflected either in clear trends in Tl fractionation, dominated by residual Tl, or in Tl speciation, dominated by Tl(I) associated with micaceous clays (Tables 1 and 2, Figure 1). This suggests that the processes resulting in the observed enrichment in the heavy ^{205}Tl in the soil horizons were linked to fractions of total soil Tl that were not readily observable in the extraction and speciation results (see the next section). The trend towards lower $\varepsilon^{205}Tl$ values, on the other hand, was reflected in higher fractions of exchangeable, oxalate-extractable and oxidizable Tl fractions in the O horizons of both profiles (Tables 1 and S5, Supplementary Material) and in the observation of hydrated Tl^+ by LCF (as well as a minor fraction of Tl(III) in sample M-Oh) (see the next section) (Table 2).

Regarding exchangeable soil Tl (NH_4NO_3-mobilizable), here we clearly detected isotopically lighter Tl in the B horizons than for the bulk soil Tl in both profiles (Tables 1 and S6, Supplementary Material), suggesting important Tl isotope shift due to the "aging" of secondary Tl (see the next section).

In soil samples from the earlier study (Voegelin et al., 2015), the measured ε^{205}Tl values ranged from +1.8 to +12.6 (Table 3) and thus spanned a larger range of Tl isotope ratios than the samples from the meadow and forest soil profiles. The lowest ε^{205}Tl value of +1.8 was measured in a Tl-rich ore fragment (P1 65 Ore R) with a predominant content of Tl(I)-jarosite (Table 3), a weathering product of primary Tl-bearing sulfide(s) (Hermann et al., 2018; Voegelin et al., 2015). The highest ε^{205}Tl values of +12.6/+12.5 were measured in two contrasting samples, a topsoil sample (P1 00-20) with relatively low Tl content mainly associated with micaceous clay minerals and a subsoil sample (P3 20-40) with much higher Tl content, with about half Tl(I) associated with micaceous clay minerals and half Tl(III) species (Table 3).

3.5 Relation of stable Tl isotope ratios to Tl fractionation, speciation, and geochemical processes

Because primary Tl-bearing sulfide minerals could not be sampled on the Erzmatt to date, the exact Tl isotopic signature of the hydrothermal mineralization is not exactly known. On the other hand, similar low ε^{205}Tl values were observed for a Tl-rich weathered ore fragment dominated by Tl(I)-jarosite (+1.8) and the bedrock sample M-R dominated by Tl(I) associated with micaceous minerals (+1.6), which may exhibit ε^{205}Tl values similar to the primary mineralization due to limited isotope fractionation during (near-quantitative) primary ore weathering. We speculate that the Tl isotopic signature of the Erzmatt mineralization could be similar to that of the Lengenbach deposit (Switzerland), which is genetically similar

to the Erzmatt except for the metamorphic processes at Lengenbach. For the Lengenbach site, Hettman et al. (2014) observed relatively low ε^{205}Tl values in sulfide and sulfosalt samples (-4.1 to +1.9), which probably resulted from isotopically light Tl in the hydrothermal fluid.

Despite the different ε^{205}Tl values of the bedrock sample (+1.6) and of the C horizon samples (+2.6/+0.8), in which Tl(I) is similarly associated with mica-type minerals, we do not expect important Tl isotopic fractionation during the (non-oxidative) Tl(I) transfer from weathering sulfide minerals (and jarosite) into pedogenic clay (Nielsen et al., 2017; Schauble, 2007). Moreover, kinetically-promoted (mass dependent) Tl isotopic fractionation during Tl sorption onto clay minerals, if present, should lead to preferential incorporation of ^{203}Tl rather than ^{205}Tl, leading to a shift to a lighter isotopic signature than in the source material (Wiederhold, 2015).

In both the meadow and forest soil profiles, ε^{205}Tl increased from the C horizons (+2.6, +0.8) to the Bw horizons (+8.7) (Figure 1, Table 1). This trend pointed to preferential accumulation of heavier ^{205}Tl as a result of soil weathering processes. Nielsen et al. (2013) document a substantial increase in the fraction of ^{205}Tl during Tl uptake by hexagonal K-birnessite; the magnitude of fractionation (α) reaching up to 1.0015 at low Tl solution concentrations where oxidative Tl sequestration was assumed to dominate Tl sorption, an assumption confirmed by recent spectroscopic work (Wick et al., 2019). This process has previously been proposed as the origin of highly-positive ε^{205}Tl anomalies in sedimentary or soil systems (Howarth et al., 2018; Kersten et al., 2014; Nielsen et al., 2013; Peacock and Moon, 2012; Rehkämper et al., 2004; Vaněk et al., 2016, 2018). Although Tl(I) may also be adsorbed non-oxidatively on Mn-oxides (Nielsen et al., 2013; Vaněk et al., 2010), non-oxidative Tl uptake is not assumed to cause substantial Tl isotopic fractionation (Nielsen et al., 2013; Schauble, 2007). The chemical extractions (oxalate-extractable Tl; reducible Tl) suggested that less than 10% of the Tl in the Bw and C horizon samples was associated with

364 Mn-oxides. Indeed, oxidative accumulation of Tl in soil Mn-concretions in the Erzmatt soil
365 samples has previously been documented using micro-XAS, but bulk XAS analyses indicated
366 that Tl-binding to Mn-oxides was quantitatively less relevant than Tl sequestration by illite
367 (or other mica-type clay minerals) (Voegelin et al., 2015). We therefore conclude that the
368 process, which resulted in the ^{205}Tl enrichment in the B horizons of the soil profiles is linked
369 to repeated Tl mobilization and immobilization processes linked to regular
370 reduction/oxidation cycles over the period of the parent rock weathering and subsequent soil
371 formation. Such a prediction favors a redoximorphic feature of the studied soils (Voegelin et
372 al., 2015). Oxidative Tl uptake associated with ^{205}Tl enrichment, continual weathering of the
373 Tl(III)-containing phases, including Mn-oxides, followed by Tl(I) remobilization (enriched in
374 ^{205}Tl) are suggested to be responsible for the migration/entry of the heavy Tl isotope fraction
375 into other phases, mainly illite. This is in line with the Tl isotopic data obtained for the
376 exchangeable soil Tl pool (Table S6, Supplementary Material), indicating preferential
377 introduction of the lighter Tl isotope fraction into "labile" soil Tl complex, and again by
378 contrast the accumulation of isotopically heavy Tl in the residual Tl pool, i.e., where Tl is
379 strongly bound (illite).

380 Although the Erzmatt soils are "young" (10,000 to 100,000 years) relative to lateritic
381 soil profiles for which redox-driven ^{205}Tl accumulation has previously been inferred (Howarth
382 et al., 2018), the process might still be fast enough relative to the period of soil formation. The
383 highest ε^{205}Tl values of +12.5/+12.6 which were measured in the sample P3 20-40 with 50%
384 Tl(III) and the sample P1 00-20 with only Tl(I)-illite (Table 3) clearly support the notion that
385 the redox Tl cycling may control the accumulation of ^{205}Tl in soil and, in parallel, also Tl(I)
386 incorporation into the pedogenic illite.

387 In both the meadow and forest soil profiles, the ε^{205}Tl value decreased from the Bw
388 over the Ah horizon to the organic soil horizons (Figure 1). The enrichment in light ^{203}Tl in

whole plants or specific plant parts relative to the substrate has already been documented (Kersten et al., 2014; Rader et al., 2019; Vaněk et al., 2019). The observed trend was therefore attributed to preferential uptake of light ^{203}Tl by plants and its accumulation in the topmost soil layers, including its binding to SOM in readily available form (Vaněk et al., 2016, 2018). Conversely, preferential uptake of ^{203}Tl by plants and its enrichment in the O and Ah horizons could also contribute to the enrichment of ^{205}Tl in the Bw horizons, in addition to ^{205}Tl enrichment due to redox-driven oxidative Tl uptake by e.g. Mn-oxides.

4. CONCLUSIONS

In this study, we combined stable Tl isotope measurements with chemical extractions and XAS speciation data to evaluate whether Tl isotopic patterns can be linked to geochemical processes present in soils (or sediments). Our results show that weathering processes/soil formation may lead to the accumulation of the heavy ^{205}Tl isotope. However, this ^{205}Tl enrichment is not reflected in changes in the Tl chemical extractability and speciation, probably because the isotopic accumulation process is complex, i.e., may be controlled by regular redox Tl cycling over the course of pedogenesis, and thus, unrelated to actual "speciation" data. This probably also allows the accumulation of ^{205}Tl in other phases, such as illite (a dominant Tl host), for which preferential uptake of ^{205}Tl is not expected. Preferential uptake of ^{203}Tl by plants and related effects on vertical enrichment and depletion of ^{203}Tl and ^{205}Tl may further complicate the situation. Accordingly, no simple correlations between Tl isotopic patterns and variations in bulk Tl chemistry and speciation can be observed.

To gain further insights into processes and mechanisms determining Tl isotopic patterns in soils, studies are required to determine the isotopic fractionation factors for individual chemical processes, such as Tl adsorption and incorporation by micaceous clay minerals, carbonates, Fe-oxides or even SOM. The question of the role or degree of these potential soil constituents in the isotopic fractionation during Tl absorption is mostly not fully clear. Therefore, the analysis and interpretation of the isotopic patterns in soils should be extended to the individual Tl host minerals/phases or well-designed chemical extracts targeting these specific Tl pools. However, for example, the approach involving redox-driven Tl mobilization with subsequent Tl isotope analysis in respective solutions, i.e., involving reductive/oxidative Tl leaching, must be omitted, since this would produce artificial isotopic fractionation unrelated to real isotopic data.

SUPPLEMENTARY MATERIAL

Detailed data on the study area and the soil sampling sites and soil profiles; supportive XRD, XANES and isotopic Tl analyses of different soil samples; a compilation of measured and reference Tl concentrations and Tl isotopic data for standard reference materials; a compilation of the physico-chemical characteristics of the studied soils and Tl, Mn and Fe concentrations and metal (mol) ratios in respective leachates from single and sequential batch extractions.

ACKNOWLEDGEMENTS

This work was funded by the Czech Science Foundation (Projects 17-03211S and 19-08614S). Part of the equipment used for this study was purchased from Operational Programme Prague – Competitiveness (Project CZ.2.16/3.1.00/21516). The Charles University team was partly supported by institutional funding from the Center for Geosphere Dynamics (UNCE/SCI/006). The Swiss Light Source (Paul Scherrer Institute, Switzerland) is acknowledged for providing the beamtime at the SuperXAS beamline. Dr. Madeleine Štulíková (a native speaker) is thanked for revision of the English manuscript. We also wish to acknowledge the anonymous three reviewers for their help with the modification of the original manuscript version.

REFERENCES

Aguilar-Carrillo, J.; Herrera, L.; Gutiérrez, E. J.; Reyes-Domínguez, I. A. Solid-phase distribution and mobility of thallium in mining-metallurgical residues: Environmental hazard implications. *Environ. Pollut.* **2018***, 243,* 1833-1845; DOI 10.1016/j.envpol.2018.10.014.

Baker, R. G. A.; Rehkämper, M.; Hinkley, T. K.; Nielsen, S. G.; Toutain, J. P. Investigation of thallium fluxes from subaerial volcanism–Implications for the present and past mass balance of thallium in the oceans. *Geochim. Cosmochim. Acta* **2009**, *73* (20), 6340-6359; DOI 10.1016/j.gca.2009.07.014.

Gomez-Gonzalez, M. A.; Garcia-Guinea, J.; Laborda, F.; Garrido, F. Thallium occurrence and partitioning in soils and sediments affected by mining activities in Madrid province (Spain). *Sci. Total Environ.* **2015**, *536*, 268-278; DOI 10.1016/j.scitotenv.2015.07.033.

Grösslová, Z.; Vaněk, A.; Oborná, V.; Mihaljevič, M.; Ettler, V.; Trubač, J.; Drahota, P.; Penížek, V.; Pavlů, L.; Sracek, O.; Kříbek, B.; Voegelin, A.; Göttlicher, J.; Ondřej, D.; Tejnecký, V.; Houška, J.; Mapani, B.; Zádorová, T. Thallium contamination of desert soil in Namibia: chemical, mineralogical and isotopic insights. *Environ. Pollut.* **2018**, *239*, 272-280; DOI 10.1016/j.envpol.2018.04.006.

Hermann, J.; Voegelin, A.; Palatinus, L.; Mangold, S.; Majzlan, J. Secondary Fe-As-Tl mineralization in soils near Buus in the Swiss Jura Mountains. *Eur. J. Mineral.* **2018**, *30*, 887-898; DOI 10.1127/ejm/2018/0030-2766.

Hettman, K.; Kreissig, K.; Rehkämper, M.; Wenzel, T.; Mertz-Kraus, R.; Markl, G. Thallium geochemistry in the metamorphic Lengenbach sulfide deposit, Switzerland: thallium-isotope fractionation in a sulfide melt. *Am. Mineral.* **2014**, *99*, 793-803; DOI doi.org/10.2138/am.2014.4591.

Howarth, S.; Prytulak, J.; Little, S. H.; Hammond, S. J.; Widdowson M. Thallium concentration and thallium isotope composition of lateritic terrains. *Geochim. Cosmochim. Acta* **2018**, *239*, 446-462; DOI 10.1016/j.gca.2018.04.017.

Jakubowska, M.; Pasieczna, A.; Zembrzuski, W.; Swit, Z.; Lukaszewski, Z. Thallium in fractions of soil formed on floodplain terraces. *Chemosphere* **2007**, *66*, 611-618; DOI 10.1016/j.chemosphere.2006.07.098.

Karbowska, B.; Zembrzuski, W.; Jakubowska, M.; Wojtkowiak, T.; Pasieczna, A.; Lukaszewski, Z. Translocation and mobility of thallium from zinc–lead ores. *J. Geochem. Explor.* **2014**, *143*, 127-135; DOI 10.1016/j.gexplo.2014.03.026.

Kersten, M.; Xiao, T.; Kreissig, K.; Brett, A.; Coles, B. J.; Rehkämper, M. Tracing anthropogenic thallium in soil using stable isotope compositions. *Environ. Sci. Technol.* **2014**, *48* (16), 9030-9036; DOI 10.1021/es501968d.

Liu, J.; Wang, J.; Chen, Y.; Xie, X.; Qi J.; Lippold, H.; Luo, D.; Wang, C.; Su, L.; He, L.; Wu, Q. Thallium transformation and partitioning during Pb − Zn smelting and environmental implications. *Environ. Pollut.* **2016**, *212*, 77-89; DOI 10.1016/j.envpol.2016.01.046.

514

515 Liu, J.; Yin, M.; Luo, X.; Xiao, T., Wu, Z.; Li, N.; Wang, J.; Zhang, W.; Lippold, H.;
516 Belshaw, N. S.; Feng, Y.; Chen, Y. The mobility of thallium in sediments and source
517 apportionment by lead isotopes. *Chemosphere* **2019**, 219, 864-874; DOI
518 10.1016/j.chemosphere.2018.12.041.

519

520 Nielsen, S. G.; Wasylenki, L. E.; Rehkämper, M.; Peacock, C. L.; Xue, Z.; Moon, E. M.
521 Towards an understanding of thallium isotope fractionation during adsorption to manganese
522 oxides. *Geochim. Cosmochim. Acta* **2013**, *117*, 252-265; DOI 10.1016/j.gca.2013.05.004.

523

524 Nielsen, S. G.; Rehkämper, M.; Prytulak, J. Investigation and application of thallium isotope
525 fractionation. *Rev. Mineral. Geochemistry* **2017**, *82*, 759-798; DOI 10.2138/rmg.2017.82.18.

526

527 Pansu, M., Gautheyrou, J. *Handbook of Soil Analysis: Mineralogical, Organic and Inorganic*
528 *Methods*; Springer-Verlag: Berlin, Heidelberg, Germany, 2006.

529

530 Peacock, C. L.; Moon, E. M. Oxidative scavenging of thallium by birnessite: Explanation for
531 thallium enrichment and stable isotope fractionation in marine ferromanganese precipitates.
532 *Geochim. Cosmochim. Acta* **2012**, *84*, 297-313; DOI 10.1016/j.gca.2012.01.036.

533

534 Peter, A. L. J.; Viraraghavan, T. Thallium: a review of public health and environmental
535 concerns. *Environ. Int.* **2005**, *31* (4), 493-501; DOI 10.1016/j.envint.2004.09.003.

536

537 Prytulak, J.; Nielsen, S. G.; Plank, T.; Barker, M.; Elliot, T. Assessing the utility of thallium
538 and thallium isotopes for tracing subduction zone inputs to the Mariana arc. *Chem. Geol.*
539 **2013**, *345*, 139-149; DOI 10.1016/j.chemgeo.2013.03.003.
540
541 Rader, S.; Maier, R. M.; Barton, M.; Mazdab, F. Uptake and fractionation of thallium by
542 Brassica juncea in geogenic thallium-amended substrate. *Environ. Sci. Technol.* **2019**, *53* (5),
543 2441-2449; DOI 10.1021/acs.est.8b06222.
544
545 Rauret, G.; López-Sánchez, J. F.; Sahuquillo, A.; Barahona, E.; Lachica, M.; Ure A. M.;
546 Davidson, C. M.; Gomez A.; Lück, D.; Bacon, M.; Yli-Halla, M.; Muntau, H.; Quevauviller,
547 Ph. Application of a modified BCR sequential extraction (three-step) procedure for the
548 determination of extractable trace metal contents in a sewage sludge amended soil reference
549 material (CRM 483), complemented by a three-year stability study of acetic acid and EDTA
550 extractable metal content. *J. Environ. Monitor.* **2000**, *2*, 228-233; DOI 10.1039/B001496F.
551
552 Rehkämper, M.; Frank, M.; Hein, J. R.; Halliday, A. Cenozoic marine geochemistry of
553 thallium deduced from isotopic studies of ferromanganese crusts and pelagic sediments. *Earth*
554 *Planet. Sci. Lett.* **2004**, *219*, 77-91; DOI 10.1016/S0012-821X(03)00703-9.
555
556 Schauble, E. A. Role of nuclear volume in driving equilibrium stable isotope fractionation of
557 mercury, thallium, and other very heavy elements. *Geochim. Cosmochim. Acta* **2007**, *71*,
558 2170-2189; DOI 10.1016/j.gca.2007.02.004.
559

560 Vaněk, A.; Grygar T.; Chrastný, V.; Tejnecký, V.; Drahota, P.; Komárek, M. Assessment of
561 the BCR sequential extraction procedure for thallium fractionation using synthetic mineral
562 mixtures. *J. Hazard. Mater.* **2010***, 176*, 913-918; DOI 10.1016/j.jhazmat.2009.11.123
563
564 Vaněk, A.; Grösslová, Z.; Mihaljevič, M.; Trubač, J.; Ettler, V.; Teper, L.; Cabala, J.;
565 Rohovec, J.; Zádorová, T.; Penížek, V.; Pavlů, L.; Holubík, O.; Němeček, K.; Houška, J.;
566 Drábek, O.; Ash, C. Isotopic tracing of thallium contamination in soils affected by emissions
567 from coal-fired power plants. *Environ. Sci. Technol.* **2016**, *50* (18), 9864-9871; DOI
568 10.1021/acs.est.6b01751.
569
570 Vaněk, A.; Grösslová, Z.; Mihaljevič, M.; Ettler, V.; Trubač, J.; Chrastný, V.; Penížek, V.;
571 Teper, L.; Cabala, J.; Voegelin, A.; Zádorová, T.; Oborná, V.; Drábek, O.; Holubík, O.;
572 Houška, J.; Pavlů, L.; Ash, C. Thallium isotopes in metallurgical wastes/contaminated soils:
573 A novel tool to trace metal source and behavior. *J. Hazard. Mater.* **2018**, *343*, 78-85; DOI
574 10.1016/j.jhazmat.2017.09.020.
575
576 Vaněk, A.; Holubík, O.; Oborná, V.; Mihaljevič, M.; Trubač, J.; Ettler, V.; Pavlů, L.;
577 Vokurková, P.; Penížek, V.; Zádorová, T.; Voegelin, A. Thallium stable isotope fractionation
578 in white mustard: Implications for metal transfers and incorporation in plants. *J. Hazard.*
579 *Mater.* **2019**, *369*, 521-527; DOI 10.1016/j.jhazmat.2019.02.060.
580
581 Voegelin, A.; Pfenninger, N.; Petrikis, J.; Majzlan, J.; Plötze, M.; Senn, A. C.; Mangold, S.;
582 Steininger, R.; Göttlicher, J. Thallium speciation and extractability in a thallium- and arsenic-
583 rich soil developed from mineralized carbonate rock. *Environ. Sci. Technol.* **2015**, *49* (9),
584 5390-5398; DOI 10.1021/acs.est.5b00629.

Wick, S.; Baeyens, B.; Marques Fernandes, M.; Voegelin, A. Thallium adsorption onto illite. *Environ. Sci. Technol.* **2018**, *52* (2), 571-580; DOI 10.1021/acs.est.7b04485.

Wick, S.; Peña, J.; Voegelin, A. Thallium sorption onto manganese oxides. *Environ. Sci. Technol.* **2019**, *53* (22), 13168-13178; DOI 10.1021/acs.est.9b04454.

Wiederhold, J. G. Metal stable isotope signatures as tracers in environmental geochemistry. *Environ. Sci. Technol.* **2015**, *49*, 2606-2624; DOI 10.1021/es504683e.

TABLES

Table 1. Total Tl concentrations (Tl_{TOT}), exchangeable (Tl_{exch}) and oxalate-extractable (Tl_{oxal}) Tl fractions, and stable Tl isotope compositions ($\varepsilon^{205}Tl$) in the studied soils and the reference material.

Profile/ Material	Sample	Tl_{TOT} (mg/kg)	Tl_{exch} (%)	Tl_{oxal} (%)	$\varepsilon^{205}Tl \pm 0.7$
Meadow	M-Oi	50.7±0.6	34.7	71.2	+3.62
	M-Oe	220±10	13.5	20.0	+4.84
	M-Ah	570±14	5.5	8.5	+7.18
	M-Bw1	657±22	5.5	7.0	+8.66
	M-Bw2	481±21	7.3	10.0	+5.57
	M-Bw3	670±12	5.0	5.9	+4.23
	M-Bw4	630±13	5.3	7.8	+3.58
	M-C	651±23	5.2	7.8	+2.60
	M-R (bedrock)	231±5	n.d.	n.d.	+1.56
Forest	F-Oi	22.1±0.5	5.3	10.8	+2.53
	F-Oe	92.9±1.3	5.8	9.8	+2.72
	F-Ah	602±25	1.9	3.8	+3.26
	F-Bw1	551±18	3.1	5.8	+8.65
	F-Bw2	526±20	4.0	5.8	+8.06
	F-Bw3	539±17	4.4	8.4	+3.63
	F-C	533±22	4.7	5.9	+0.76
AGV-2		0.25	n.d.	n.d.	-2.57

The uncertainties for total Tl concentrations are reported at the 2 SD level (n = 3). The relative data on exchangeable (1 M NH_4NO_3) and oxalate-extractable Tl are the means (n = 3) with RSD <10%. The $\varepsilon^{205}Tl$ results are assigned an error of ± 0.7 $\varepsilon^{205}Tl$ (2 SD), based on the long-term reproducibility of multiple separate analyses (involving sample digestion, column chemistry and mass spectrometry) of standard reference material AGV-2 (Andesite, USGS, USA) (3 for this study) (Table S2, Supplementary Material). n.d.: not determined.

Table 2. Linear combination fit analysis of Tl L_{III}-edge XANES spectra of meadow and forest soil samples. The sample and reconstructed LCF spectra are shown in Figures 2 and S5 (Supplementary Material). In the LCF, Tl_2O_3 represents Tl(III) in organic or inorganic form, aqueous Tl^+ represents hydrated Tl^+ sorbed on the soil (mineral/organic) components or in the biomass, and soil sample M-C represents Tl(I) in micaceous clay minerals (see text for details).

Sample	Tl_2O_3	aq. Tl^+	M-C	sum	NSSR[a]
M-Oi	0.08	0.66	0.25	0.99	0.00110
M-Oe	--	0.37	0.63	1.00	0.00020
M-Ah	--	--	1.00	1.00	0.00007
M-Bw2	--	--	1.00	1.00	0.00016
F-Oi	--	0.11	0.88	1.00	0.00058
F-Oe	--	--	1.00	1.00	0.00009
F-Ah	--	--	1.00	1.00	0.00020
F-Bw2	--	--	1.00	1.00	0.00012
F-C	--	--	1.00	1.00	0.00018

[a]NSSR = normalized sum of squared residuals ($\sum(data_i\text{-}fit_i)^2/\sum data_i^2$).

695 **Table 3.** Total Tl concentrations (Tl_{TOT}) and LCF-derived Tl speciation in selected samples
696 from Voegelin et al. (2015) and corresponding stable Tl isotope data ($\varepsilon^{205}Tl$).
697
698

Sample	Tl_{TOT} (mg/kg)	Tl(I)-illite	Tl(I)-jarosite	Tl(III)	$\varepsilon^{205}Tl \pm 0.7$
P1 00-20	119	1.00	--	--	+12.63
P1 20-40	265	0.93	--	0.07	+6.44
P1 60-80	1801	0.32	0.32	0.36	+5.27
P1 65 Ore R	5677	--	0.84	0.17	+1.76
P1 95-115	1120	--	0.48	0.52	+6.01
P2 00-20	438	0.82	0.11	0.07	+7.41
P2 44-64	981	0.46	0.36	0.19	+6.74
P2 60-80	706	0.84	0.16	--	+6.18
P2 95-115	151	1.00	--	--	+7.76
P3 00-20	1142	0.87	--	0.13	+9.78
P3 20-40	3269	0.43	--	0.57	+12.49

699
700 Sample names indicate profile number (n = 3) and sampling depth (interval). The samples are
701 averaged bulk samples, except sample P1 65 Ore R, a red weathered ore fragment.

FIGURE CAPTIONS

Figure 1. Vertical evolution of total (Tl_{TOT}), exchangeable and oxalate-extractable Tl concentrations, chemical Tl fractionation (≤25% of total fractionation) and Tl isotopic compositions ($\varepsilon^{205}Tl$) in the studied soils – (M) meadow, (F) forest.

Figure 2. Tl L_{III}-edge XANES spectra of selected soil samples from the meadow profile (M-Oi, M-Oe, M-Ah, M-Bw2, M-C) and reference spectra $Tl^{III}_2O_3$ (Voegelin et al., 2015), proxy for Tl(III); aqueous Tl^+ (Wick et al., 2018), proxy for hydrated Tl^+; Tl^I-illite (sample with 3800 mg/kg Tl) (Wick et al., 2018), proxy for Tl(I) adsorbed at frayed edge sites or bound in the interlayer of micaceous clay minerals. The gray dashed lines in the right panel represent linear reconstruction spectra based on the LCF results in Table 2. The spectra of selected samples from the forest profile are available in the Figure S5 (Supplementary Material).

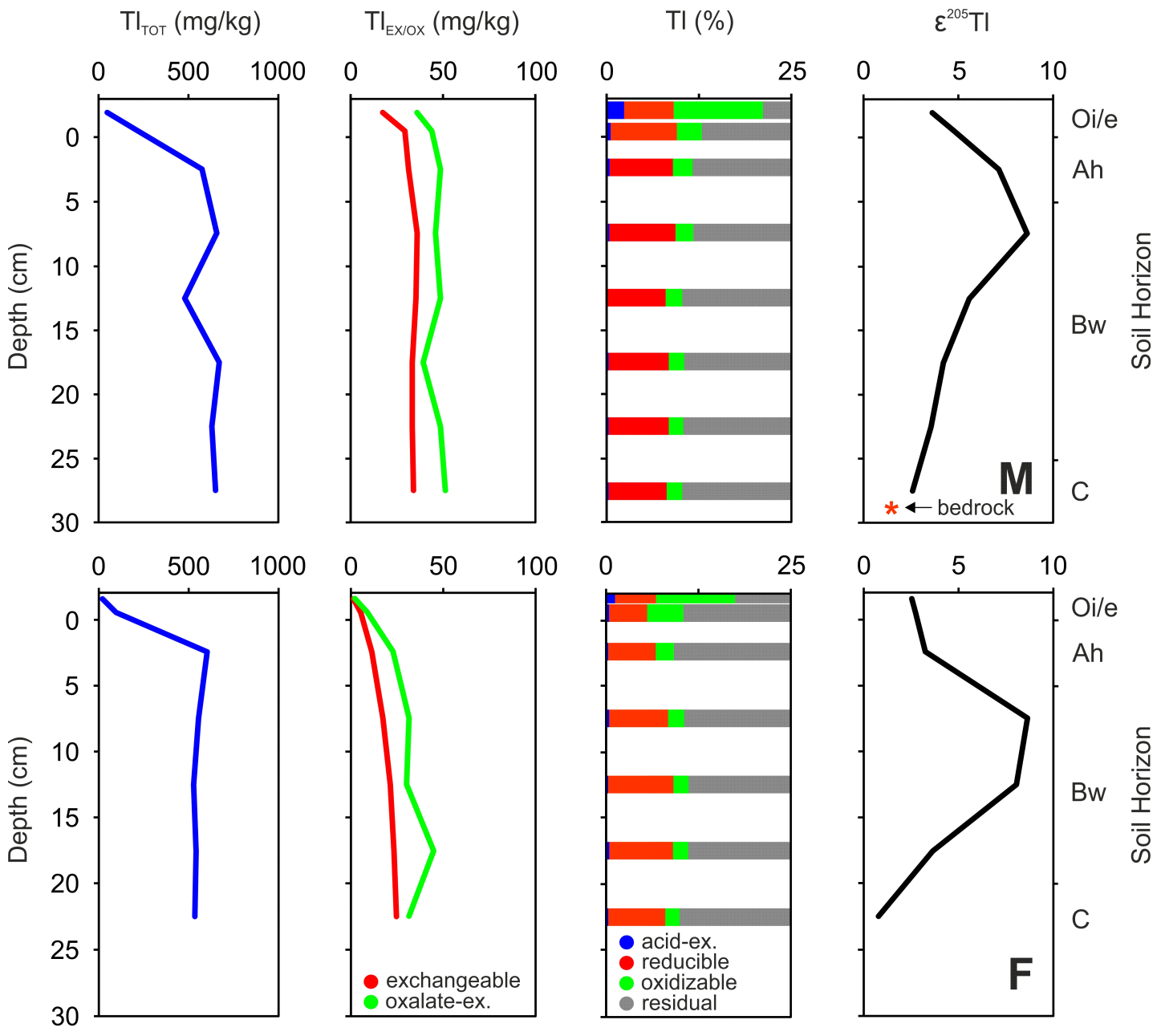
Tl$_{TOT}$ (mg/kg)
Tl$_{EX/OX}$ (mg/kg)
Tl (%)
ε^{205}Tl
0
500
1000
50
100
25
5
10
Depth (cm)
0
5
10
15
20
25
30
Oi/e
Ah
Bw
C
Soil Horizon
M
bedrock
F
exchangeable
oxalate-ex.
acid-ex.
reducible
oxidizable
residual

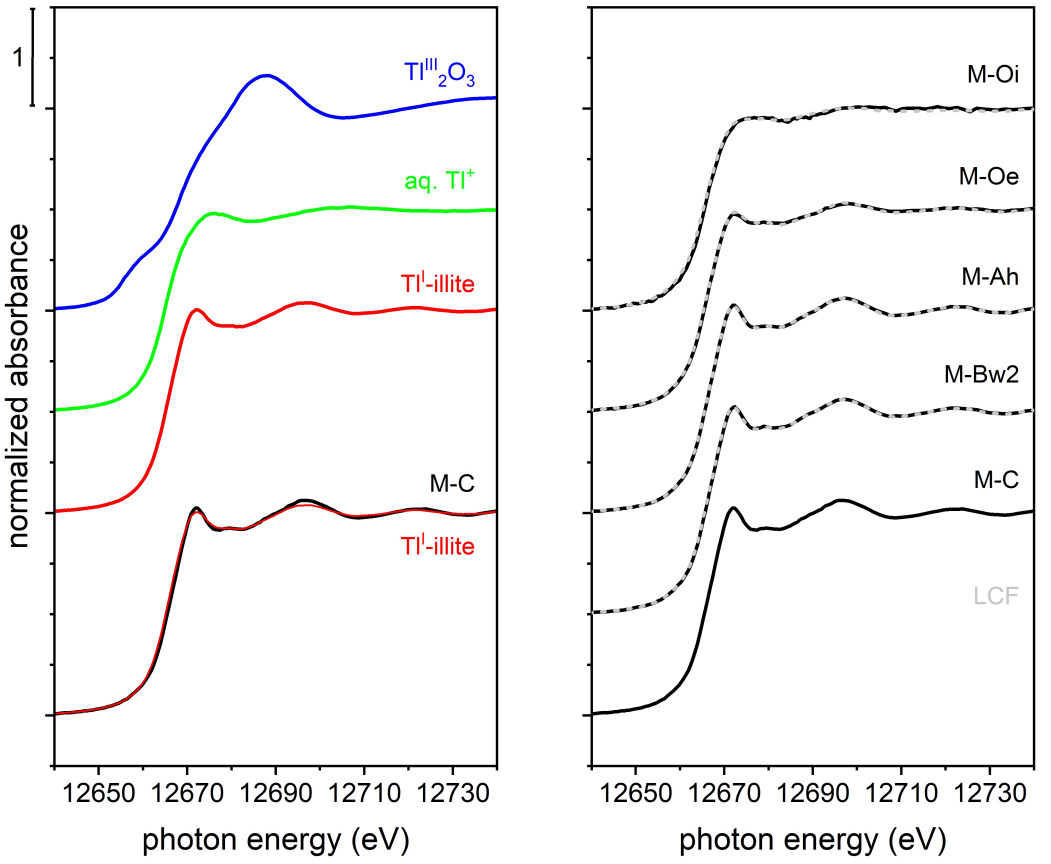
1
normalized absorbance
$Tl^{III}_2O_3$
aq. Tl^+
Tl^I-illite
M-C
Tl^I-illite
12650 12670 12690 12710 12730
photon energy (eV)
M-Oi
M-Oe
M-Ah
M-Bw2
M-C
LCF
12650 12670 12690 12710 12730
photon energy (eV)